

Level crossing of particle-hole and mesonic modes in eta mesic nuclei

D. Jido ^a, E.E. Kolomeitsev ^{b,a,c}, H. Nagahiro ^d, S. Hirenzaki ^e

^a*Yukawa Institute for Theoretical Physics, Kyoto University, Kyoto 606-8502, Japan*

^b*School of Physics and Astronomy, University of Minnesota, 116 Church Str SE, Minneapolis 55455, USA*

^c*Gesellschaft für Schwerionenforschung (GSI), Planck Str. 1, 64291 Darmstadt, Germany*

^d*Research Center for Nuclear Physics (RCNP), Osaka University, Ibaraki, Osaka 567-0047, Japan*

^e*Department of Physics, Nara Women's University, Nara 630-8506, Japan*

Abstract

We study eta meson properties in the infinite nuclear matter and in atomic nuclei with an emphasis on effects of the eta coupling to $N^*(1535)$ -nucleon-hole modes. The $N^*(1535)$ resonance, which dominates the low-energy eta-nucleon scattering, can be seen as a chiral partner of the nucleon. The change of the chiral mass gap between the N^* and the nucleon in a nuclear medium has an impact on the properties of the eta-nucleus system. If the N^* -nucleon mass gap decreases with a density increase (chiral symmetry restoration) the calculations show the existence of the resonance state at the energy about 60 MeV and two bound eta-nucleus states with the binding energies about -80 MeV. These states can have strong effect on predicted cross sections of the $^{12}\text{C}(\gamma, p)^{11}\text{B}$ reaction with eta-meson production.

Key words:

eta mesic nucleus, energy dependent potential, chiral symmetry, chiral doublets, $N(1535)$, eta nucleon interaction,

PACS: 21.65.-f, 21.65.Jk, 21.85.+d, 14.40.Aq, 14.20.Gk, 11.30.Rd, 12.39.Fe,

1 Introduction

The eta bound states in nuclei were theoretically predicted by Haider and Liu [1]. This prediction relied on the first estimation of the ηN interaction

just made that time by Bhalerao and Liu [2], who obtained an attractive ηN scattering length. Being electrically neutral the eta meson can be bound only by strong interactions. Simultaneously, the strong interactions induce nuclear absorption of the bound eta meson, which wave function has to have large overlap with a nucleus. As the result the position and the width of the bound level are determined by a complicated interplay of the nuclear density distribution and the strength of the in-medium ηN interaction. Therefore the experimental proof of the existence of eta bound states could provide information on modification of meson properties in nuclear matter complimentary to that obtained from pionic and kaonic atoms [3]. Particularly, the existence of such states in light nuclei would set important constraints [4]. Currently, various theoretical calculations predict the natural widths of eta bound states to be larger than the level spacing [5,6,7,8,9,10,11,12]. This could explain problems in experimental identification of the eta bound states.

The first experimental search for eta bound states in (π^+, p) reactions [13] gave a negative result as being aimed only at the narrow states as it was proposed in Ref. [1]. At the same time the measured excitation functions for reactions $d(p, {}^3\text{He})\eta$ [14] and ${}^{18}\text{O}(\pi^+, \pi^-){}^{18}\text{Ne}$ [15] showed some enhancement near the η production threshold which could be a hint for a bound state. Sokol and Triasuchev argued in [16] that the eta bound state can be more easily identified if one tags on the $N(1535)$ resonance in the final state by observing its π^+n decay. Such an identification method was realized in experiments at the Lebedev Physical Institute studying (γ, p) reaction on the ${}^{12}\text{C}$ target. The observed enhancement of π^+n production occurring when the photon energy exceeds the eta production threshold can be interpreted as a signal of η -nucleus formation [17]. Observation of an eta bound state in ${}^3\text{He}$ with the binding energy (-4.4 ± 4.2) MeV and the full width (25.6 ± 6.1) MeV in photoproduction reactions at MAMI was reported in [18]. The bound state was identified by registration of two decay modes with an explicit eta in the final state and with $\pi^0 p$. Interpretation of these experimental results in terms of the eta bound state was, however, questioned in [19]. A new support for $\eta^3\text{He}$ bound state arises from the recent study of $d p \rightarrow {}^3\text{He} \eta$ reaction at COSY [20]. Other experiments have been proposed for searching eta bound states [21,22,23].

Proton pickup processes are powerful experimental tools for studying light mesons in nuclei. They allow for the recoilless creation of a meson inside a nucleus by fine tuning the energy of an incident particle. It is well-known, e.g., that the $(d, {}^3\text{He})$ reactions on nuclear targets lead to formation and identification of the deeply bound pionic atoms [24,25,26,27]. The (γ, p) and (π, p) reactions have also been proposed as good experimental tools for formation of eta-nucleus systems. In the recoilless production, the eta meson is created almost at rest and may be absorbed within the nucleus. Although the eta meson is not directly observed in the final states, we can extract properties

of the eta-nucleus system by measuring of the production cross section as a functions of the momentum of the emitted particle [7,10,11,12]. Thereby one has access to the energies corresponding to eta mesons bound in nuclei. This is one of the differences from the eta production reactions on nuclear targets, where the eta meson emitted from the nucleus is observed [28,29,30].

The prominent feature of the eta meson is that the eta-nucleon system couples dominantly to the $N^*(1535)$ (S_{11}) resonance at threshold energies [31]. The ηNN coupling is, on the contrary, much smaller than ηNN^* and πNN ones [32] and is basically irrelevant for analyses of the NN scattering and the threshold η production on a nucleon [2,33]. Therefore the low-momentum eta meson would dominantly excite N^* -nucleon-hole ($N^* - h$) states in nuclear medium. The difference between the eta mass and the $N^* - N$ mass gap is just 50 MeV, which is smaller than the N^* width $\Gamma_{N^*} \simeq 75$ MeV and is comparable with the depth of the attractive potential acting on the nucleon in a nucleus, $\sim 50 - 60$ MeV. Hence, one could expect the eta meson nuclear dynamics to be sensitive to modifications of nucleon and N^* properties in medium.

The question about in-medium dynamics of the $N(1535)$ resonance addresses an interesting aspects of the chiral symmetry of strong interactions. Being the lowest lying baryon with the opposite parity to the nucleon, the $N(1535)$ can be viewed as its chiral partner [34,35,36,37,38]. Analogously one considers pairs (σ, π) and (ρ, a_1) . If now the chiral symmetry is getting restored with an increasing baryon density the parity partners will become degenerate. This picture has several interesting phenomenological consequences [34,35,38]. The important implication for the eta meson physics is that the $N - N^*$ mass gap decreases in nuclear medium and at some density goes below the η mass [39,36]. This changes the sign of the η meson optical potential making it repulsive at saturation density as found in [10,11,12].

The parity-doublet concept corresponds to a linear realization of chiral symmetry in terms of hadrons. In a non-linear realization the parity partner is not present in the Lagrangian as an independent degree of freedom but rather manifests itself as a pole of the scattering amplitude generated dynamically by coupled channels. So, the $N^*(1535)$ can be viewed as a $K\Sigma$ and $K\Lambda$ quasi-bound state [40,41,42,43]. In general the dynamically generated states could be very sensitive to in medium modifications of the meson-baryon loops they are made of. For instance the dynamically generated $\Lambda(1405)$ resonance would dissolve or become very broad in nuclear medium [44,45,46,47]. In the case of the $N^*(1535)$ the in-medium modification of kaon-hyperon loops is expected to be smaller [44,48] since there is no Pauli blocking for hyperons and K mesons interact rather weakly with nucleons. However, even in this case both hyperons and nucleons can couple to an attractive scalar nuclear mean field, which is responsible for a decrease of baryon masses in nuclear matter. Thus, the shift of the N^* with respect to the nucleon depends on how strongly hyperons

and nucleons couple to the scalar field. If the couplings are equal then the N and N^* masses decrease roughly in the same manner that keeps the $N^* - N$ mass gap constant. It is known, however, from physics of hypernuclei that the hyperons are bound weaker than nucleons. This could lead to an increase the $N^* - N$ mass gap in the nuclear medium.

As discussed above, these two different pictures for $N(1535)$ imply distinct phenomenological consequences for eta meson dynamics in the nuclear matter [11,12]. In the parity-doublet model the eta optical potential is shallower, that reduces the binding [10,11,12].

Typically, calculations done in previous works operated with energy-independent optical potentials. In the case when $N^* - N$ gap becomes close to or smaller than the eta mass it is not a reliable approximation anymore, and the energy dependence must be taken into account explicitly. The eta meson quantum numbers can be carried now not only by the eta-particle modes but also by the N^* -nucleon-hole modes. In the present paper we study the propagation of these modes in nuclear matter and finite nuclei. We discuss a possibility of the formation of an “eta nucleus” by $N^* - h$ modes¹.

In Section 2 we construct the eta meson Green function in nuclear matter exploiting the N^* dominance in the ηN scattering. We calculate the spectrum of eta excitations in the infinite nuclear system and analyze how the eta spectral density changes with the nuclear matter density. Section 3 is devoted to eta excitations in finite nuclei. First we discuss the spectral function convoluted with the density distribution in ^{11}B . This gives an approximate view on how the nucleus would respond to the external source with the eta quantum numbers. For better understanding the observed bump structures we solved the Lippmann-Schwinger equation for the eta-nucleus scattering amplitude in the momentum representation and identify poles of the amplitude on the complex energy plane. In Section 4 we calculate missing mass spectra in the (γ, p) reaction on ^{12}C target associated with the eta meson formation.

2 Eta meson in nuclear matter

2.1 Eta self-energy in nuclear matter

In this section we investigate the eta meson in infinite uniform nuclear medium. The propagation of the eta meson is described in terms of the in-medium Green

¹ Similar interpretation of the “eta nucleus” in terms of both eta-particle and resonance-hole modes was proposed in [16].

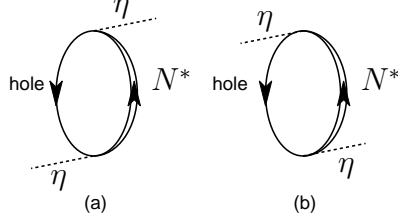


Fig. 1. Diagrams for the η self-energy in the nuclear matter. (a) and (b) are the direct and crossing diagrams, respectively.

function with the self-energy $\Pi_\eta(\omega, k; \rho)$

$$G_\eta(\omega, k; \rho) = \frac{1}{\omega^2 - k^2 - m_\eta^2 - \Pi_\eta(\omega, k; \rho) + i\epsilon}. \quad (1)$$

Here ω and k denote the eta energy and momentum, ρ is the nuclear density, and m_η is the vacuum eta mass. We consider the isospin symmetrical nuclear matter.

The eta nucleon interaction is dominated by the N^* resonance which contributes to the s-wave scattering amplitude. The higher partial waves are less important for slow η mesons created in reactions at recoilless conditions. Thus, the main contribution to the eta self-energy is due to the excitations of N^* -nucleon-hole modes as shown in Fig. 1. Exactly these diagrams induce the strong energy dependence of the self-energy.

The ηNN^* coupling is defined by the Lagrangian

$$\mathcal{L}_{\eta NN^*} = g (\bar{N} N^* + \bar{N}^* N) \eta, \quad (2)$$

where the coupling g can be estimated as $g \simeq 2$ from the vacuum $N^* \rightarrow \eta N$ decay width

$$\Gamma_{N^* \rightarrow \eta N} = g^2 \frac{(m_{N^*} + m_N)^2 - m_\eta^2}{16 \pi m_{N^*}^3} \sqrt{(m_{N^*}^2 - m_N^2 - m_\eta^2)^2 - 4 m_N^2 m_\eta^2},$$

with the vacuum values, $\Gamma_{N^* \rightarrow \eta N} \simeq 75$ MeV, $m_N = 939$ MeV, $m_{N^*} = 1535$ MeV and $m_\eta = 547$ MeV.

In the gas approximation the self-energy depicted in Fig. 1 reads

$$\Pi_\eta(\omega, k; \rho) = \frac{g^2 \rho}{\omega - (m_{N^*}^*(\rho) - m_N^*(\rho)) - \frac{k^2}{2m_{N^*}^*} + i \Gamma_{N^*}(\omega; \rho)/2}$$

$$+ \frac{g^2 \rho}{-\omega - (m_{N^*}^*(\rho) - m_N^*(\rho)) - \frac{k^2}{2m_{N^*}^*}}, \quad (3)$$

where the first and second terms in Eq. (3) correspond to the diagrams (a) and (b) in Fig. 1, respectively. We neglect here momenta of the nucleon and the N^* . The linear density dependence in the numerator of Eq. (3) is obtained by the Fermi momentum integration over the nucleon hole state. The density-dependent in-medium masses of the N^* and N are denoted as $m_{N^*}^*(\rho)$ and $m_N^*(\rho)$, respectively. $\Gamma_{N^*}(\omega; \rho)$ is the in-medium N^* width determined by the N^* self-energy, $\Gamma_{N^*}(\omega; \rho) = -2 \Im \Sigma_{N^*}(m_{N^*}^*(\rho) + \omega; \rho)$. There is no width in the second term in Eq. (3) since $\Im \Sigma_{N^*}(m_N^*(\rho) - \omega; \rho) = 0$.

Below we use the chiral doublet model [38] for the medium modification of the N and N^* masses. In this model, the mass difference of the nucleon and N^* is determined by the chiral condensate $\langle \sigma \rangle$ as

$$m_{N^*}^*(\rho) - m_N^*(\rho) = A \langle \sigma \rangle \quad (4)$$

with the parameter $A = (m_N - m_{N^*}) / \langle \sigma \rangle_0$, where $\langle \sigma \rangle_0$ is the vacuum chiral condensate. Assuming a partial restoration of chiral symmetry in the nuclear medium and parameterizing of the sigma condensate as a function of the nuclear density [49], $\langle \sigma \rangle = (1 - C \rho / \rho_0) \langle \sigma \rangle_0$, we obtain the in-medium mass difference

$$m_{N^*}^*(\rho) - m_N^*(\rho) = (m_{N^*} - m_N)(1 - C \rho / \rho_0). \quad (5)$$

The parameter C represents the strength of chiral restoration at the normal density and its reasonable values are in the range of $C = 0.1$ – 0.3 . The value of the C parameter can be evaluated within the chiral doublet model providing $C \simeq 0.22$, which is read off the density dependence of the chiral condensate calculated in Ref. [39]. In this paper we use $C = 0.2$ [10,11,12]. The mass of the eta meson is assumed to be constant in the nuclear medium [50,51] (no scalar mean-field potential).

There are several contributions to the imaginary part of the N^* self-energy, among which the main modes are the pionic decay, $N^* \rightarrow \pi N$, and the two-body absorption, $N^* N \rightarrow \pi N N$ [6,10]. The decay process $N^* \rightarrow \eta N$ is forbidden in nuclear matter due to the Pauli blocking. The width of $N^* \rightarrow \pi N$ reaction calculated in Ref. [39] within an improved parity-doubled model is depicted in Fig. 2 (dashed lines) as a function of the energy for different nucleon densities. The steep rise of the width is due to the pseudoscalar $\pi N^* N$ coupling motivated by the chiral symmetry. For $C = 0.2$ this partial width is decreasing with a growing density as the chiral symmetry is getting restored and pions decouple from baryons. For $C = 0.0$ the width $\Gamma_{N^* \rightarrow \pi N}$ does not

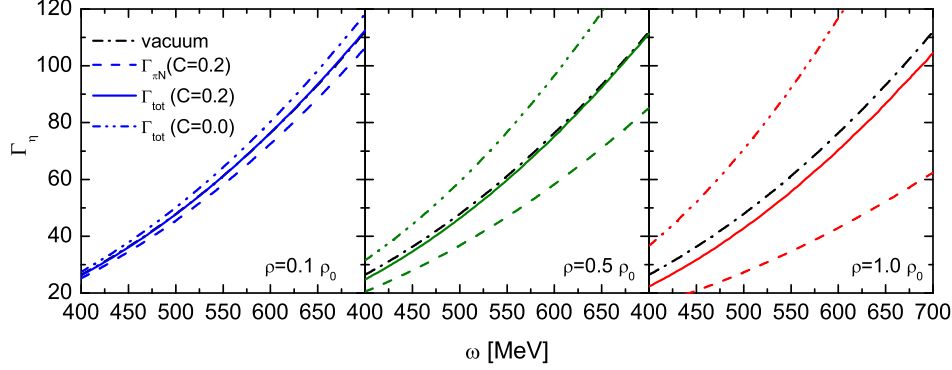


Fig. 2. Energy dependence of the N^* widths: the partial width $\Gamma_{N^* \rightarrow \pi N}$ (dashed lines) and the total width $\Gamma_{N^*} \approx \Gamma_{N^* \rightarrow \pi N} + \Gamma_{N^* N \rightarrow NN\pi}$ calculated for $C = 0.2$ (solid lines) and $C = 0.0$ (dash-dot-dot lines) are shown for different values of the nucleon densities. Dash-dot lines show the vacuum $\Gamma_{N^* \rightarrow \pi N}$ width. For $C = 0.0$ the partial width $\Gamma_{N^* \rightarrow \pi N}$ coincides with the vacuum one.

$a_{\eta N}$ [fm]	$0.55 + i 0.39$	$0.20 + i 0.26$	$0.26 + i 0.25$	$0.27 + i 0.22$
Ref.	this work	[41]	[43]	[2]
$a_{\eta N}$ [fm]	$0.51 + i 0.21$	$0.55 \pm 0.02 + i 0.3$	$0.88 + i 0.27$	$0.98 + i 0.37$
Ref.	[52]	[53]	[54]	[55]

Table 1

Summary of the values of the ηN scattering length.

depend on the density. The $N^* N \rightarrow \pi NN$ reaction has been calculated in Ref. [10]. The total N^* width is depicted in Fig. 2 by solid lines for $C = 0.2$ and by dash-dot-dot lines for $C = 0.0$. The analysis done in this section for the case of the homogeneous nuclear matter shows that, in principle, it is sufficient to take density and energy independent value for the total width Γ_{N^*} given by the vacuum value $\Gamma_{N^* \rightarrow \pi N} = 75$ MeV. Later in the calculation of the formation spectra of the eta-nucleus system, we will use more realistic N^* decay widths reported in Refs. [10,11,58].

We should verify how our model describes the low energy ηN interaction. The ηN scattering amplitude can be related to the η self-energy as $T_{\eta N}(\omega, k) = -\partial \Pi_{\eta}(\omega, k; \rho) / \partial \rho \Big|_{\rho=0}$. Using this relation, we calculate the ηN scattering length

$$a_{\eta N} = \frac{T_{\eta N}(m_{\eta}, 0)}{4\pi(1 + m_{\eta}/m_N)} \simeq 0.55 + i 0.39 \text{ fm}. \quad (6)$$

Note that $\Gamma_{\eta N}(\omega = m_{\eta}) = 0$, since the $N^* \rightarrow \eta N$ channel is closed at the threshold. The values reported in the literature are summarized in Table 1. Our value of the scattering length is consistent with the other model calculations.

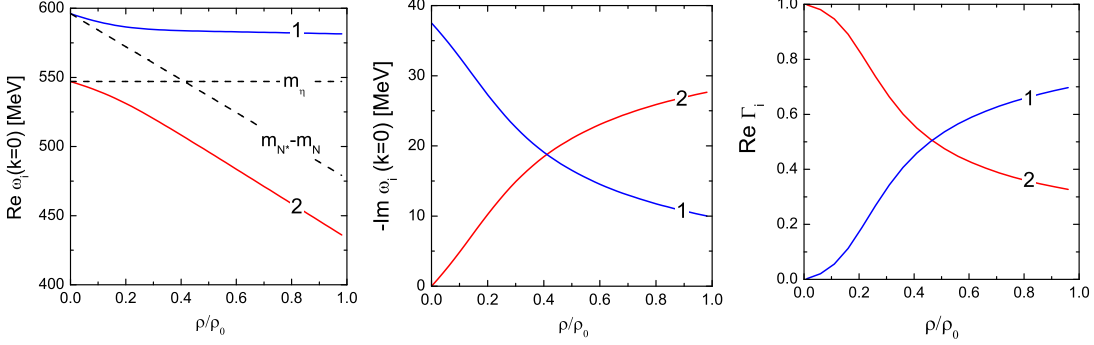


Fig. 3. The real (left panel) and imaginary (middle panel) parts of the solutions, ω_i , of eq. (8) and the occupations factors (9) (right panel) for vanishing momentum as functions of the baryon density. The dashed lines on the left panel denote the eta and N^* - h modes without the channel mixing ($g = 0$). Calculations are done for $C = 0.2$.

With the positive ηN scattering length, the ηN interaction is attractive at the threshold. Thus, the self-energy of the eta meson is also attractive at low densities and $\omega \simeq m_\eta$. This attraction is due to the N^* resonance above the ηN threshold. Indeed, since the vacuum masses of η , N and N^* satisfy $m_\eta < m_{N^*} - m_N$, the real part of the self-energy has a negative value at $\omega \simeq m_\eta$. At moderate densities when medium effects for the N and N^* are not so strong and the inequality $m_\eta < m_{N^*}(\rho) - m_N(\rho)$ still holds, the optical potential of the eta meson remains attractive for $\omega \simeq m_\eta$. If some medium effects and/or a density increase bring the $N^* - h$ state down below the eta state, so that $m_\eta > m_{N^*}(\rho) - m_N(\rho)$, the real part of the self-energy turns to be positive and the optical potential of the eta meson becomes repulsive [10,11,12]. Therefore, the order of mesonic and particle-hole levels determines the sign of the self-energy, once two modes couple. Furthermore, the level difference between these modes is only about 50 MeV. Hence, the self-energy of the eta meson is very sensitive to the in-medium properties of the N and N^* masses. In addition, the level coupling brings strong energy dependence to the self-energy. Therefore it may be wrong to discuss the eta meson in nuclear medium in terms of an energy-independent optical potential. In the next subsection, we discuss the spectrum of eta modes propagating in nuclear medium taking into account this energy dependence.

The above discussion is quite general and does not depend on details of the mechanism of the N and N^* mass reduction.

2.2 Eta spectrum in the nuclear matter

In this section we investigate the spectral function of the eta meson in the infinite nuclear medium.

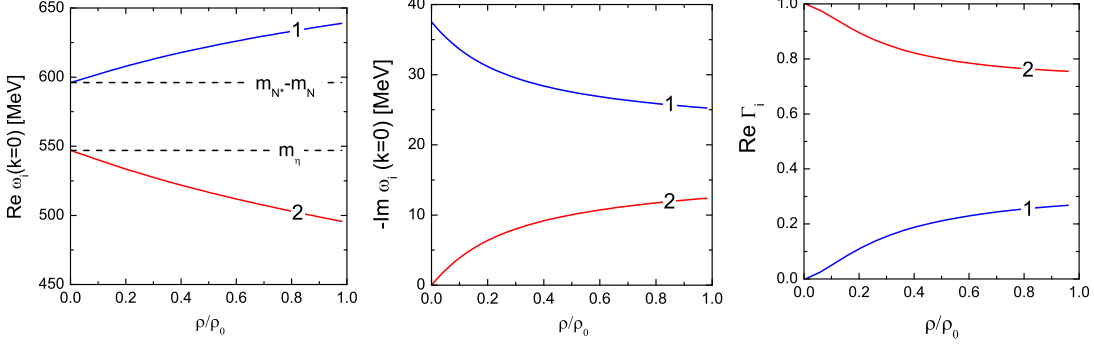


Fig. 4. The same as in Fig. 3 but calculated with $C = 0$.

The full in-medium propagator of the eta meson (1) can be decomposed as

$$G_\eta(\omega, k; \rho) = \sum_i \frac{\Gamma_i(k; \rho)}{\omega - \omega_i(k; \rho)}, \quad (7)$$

where ω_i 's are complex numbers being the solutions of the Dyson equation $G_\eta^{-1}(\omega, k; \rho) = 0$ with the self-energy (3):

$$\omega^2 - k^2 - m_\eta^2 - g^2 \rho \frac{2\omega_R(k; \rho) - i\Gamma_{N^*}/2}{[\omega - \omega_R(k; \rho) + i\Gamma_{N^*}/2][\omega + \omega_R(k; \rho)]} = 0. \quad (8)$$

We denote here $\omega_R(k; \rho) = m_{N^*}^*(\rho) - m_N^*(\rho) + k^2/(2m_{N^*}^*(\rho))$. This equation has two complex solutions with a positive real part, $\omega_i(k)$, $i = 1, 2$. These solutions describe two branches² of the η -meson spectrum in nuclear matter³. They are shown in Fig. 3 by solid lines for $k = 0$ as functions of the baryon density. With the vanishing coupling constant g the eta-meson mode and N^* -nucleon-hole mode are decoupled and only the mesonic mode can carry the η quantum numbers. This case is depicted by the dashed lines on the left panel in Fig. 3. The modes cross each other at $\rho \simeq 0.4\rho_0$ for $k = 0$. The finite value of the coupling g leads to the avoided level crossing and the redistribution of the eta quantum numbers between both branches.

The residues of the poles of the propagator $G_\eta(\omega, k)$ at $\omega = \omega_i$ quantify the occupation of each branch by the eta-meson quantum numbers:

$$\Gamma_i(k; \rho) = 2m_\eta Z_i(k; \rho), \quad Z_i(k; \rho) = \left(2\omega - \frac{\partial \Pi_\eta(\omega, k; \rho)}{\partial \omega}\right)^{-1} \Big|_{\omega=\omega_i(k)}. \quad (9)$$

² For the first time the two-branch spectrum of eta mesons in nuclear matter has been discussed in Ref. [56].

³ In general case the assignment of different solutions of the Dyson equation to the in-medium branches of particles and anti-particles should be done according to the sign of the real parts of the residues, cf. [57]

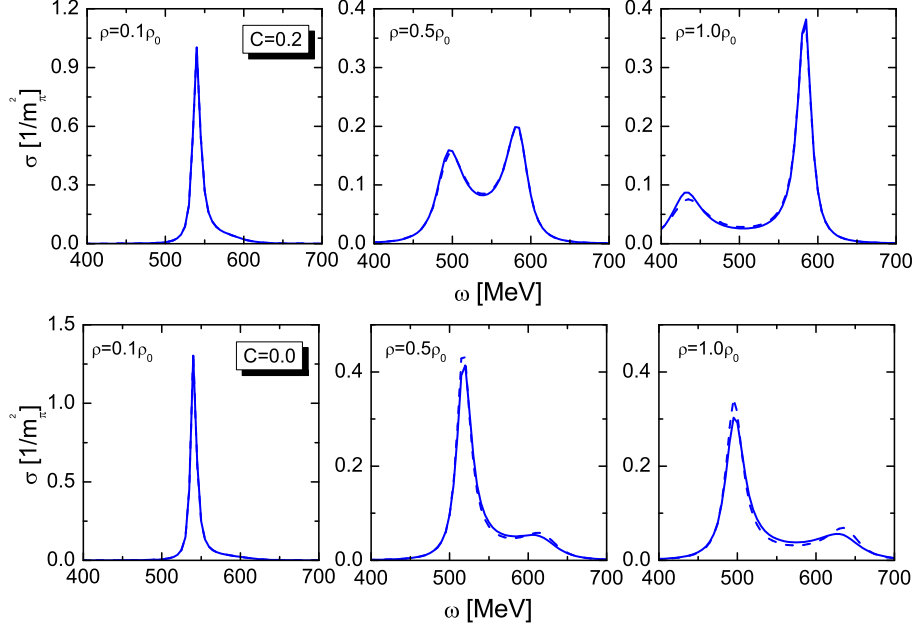


Fig. 5. The η meson spectral density (10) in nuclear matter at densities $0.1\rho_0$, $0.5\rho_0$ and $1\rho_0$ for the vanishing momentum. Dashed lines are calculated with the constant N^* width $\Gamma_{N^*} = 75$ MeV. The solid lines show the results with the energy and density dependent width shown in Fig. 2. The upper row is calculated with $C = 0.2$ and the lower one with $C = 0$.

Note, it is important to include the imaginary part γ_i by evaluating Z -factors. Then they have the following property $\Im Z_1(k) + \Im Z_2(k) \simeq 0$ and $\Gamma_1(k; \rho) + \Gamma_2(k; \rho) = 1$. The dependence of the occupation factors on the nucleon density is shown on the right panel in Fig. 3. We see that at $\rho < 0.4\rho_0$ the eta quantum numbers populate dominantly branch 2 and for $\rho > 0.4\rho_0$ branch 1.

In order to illustrate the effects of the chiral symmetry restoration we depict in Fig. 4 the same eta spectrum parameters as in Fig. 3 but calculated for $C = 0$. The mass gap of branch 1, $\omega_1(k=0)$, increases now with the increasing density and that of branch 2 decreases half as strong as for $C = 0.2$. The occupation factors show that branch 2 carries now the dominant part of the eta mesons.

The spectral function is defined by the imaginary part of the full propagator (1):

$$\sigma(\omega, k; \rho) = -\frac{1}{\pi} \Im G_\eta(\omega, k; \rho). \quad (10)$$

In Fig. 5 the spectral density is shown for several values of the nucleon density at the vanishing momentum. At lower density ($\rho = 0.1\rho_0$) there is one peak, which corresponds to the eta mesonic mode. At higher densities a two-peak structure emerges. The second peak comes from the N^* - h mode which couples to the eta mode in nuclear medium. The coupling strength increases as the

density increases. The dashed curves are calculated with the constant N^* width $\Gamma_{N^*} = 75$ MeV. The solid curves are calculated with the full energy and density dependent N^* width depicted in Fig. 2. We note that dashed and solid curves coincide almost perfectly. For $C = 0$ the low-energy peak of the spectral density is stronger pronounced than for $C = 0.2$ though it is located at somewhat higher energies. It is interesting to see how these differences in the spectral function reveal themselves in the finite nuclear systems and in eta production reactions.

3 Eta meson modes in finite nuclei

3.1 Density-averaged spectral function

In eta production reactions on finite nuclei the spectral function (10) is probed at different densities which produce superposed contributions to the observed final signal. Therefore, in order to get a feeling on the response of a nucleus to an external source with the eta-meson quantum numbers its instructive to study the spectral function averaged over the density distribution in a nucleus:

$$\bar{\sigma}(\omega, k) = -\frac{4}{A} \int dr r^2 \rho(r) \Im G_{\eta}(\omega, k; \rho(r)). \quad (11)$$

Here $\rho(r)$ is a spatial distribution of the nucleon density in a nucleus normalized to the total number of nucleons $A = 4\pi \int dr r^2 \rho(r)$. We use the 2-parameter Fermi distribution:

$$\rho(r) = \frac{\rho_0}{1 + \exp\left(\frac{r-R}{a}\right)}. \quad (12)$$

For ^{11}B , which is the remaining nucleus for eta production reactions on ^{12}C , we have the central density $\rho_0 = 0.173 \text{ fm}^{-3}$, the nuclear radius $R = 1.18A^{1/3} - 0.48 = 2.14 \text{ fm}$ and the diffuseness parameter $a = 0.5 \text{ fm}$.

In Fig. 6 we plot the density-averaged nuclear response functions (11) with $C = 0.0$ and $C = 0.2$. Recalling the in-medium spectral function shown in Fig. 5, we find the following correspondence between the structures in these two response functions: the pronounced cusp structure at the eta production threshold corresponds to lower densities, when the eta is produced at the surface of the nucleus, and medium effects are small as seen on the left panel in Fig. 5. Two bumps — one in the continuum region ($E > 0$) and the other one in the bound regions ($E < 0$) — correspond to the two modes in the

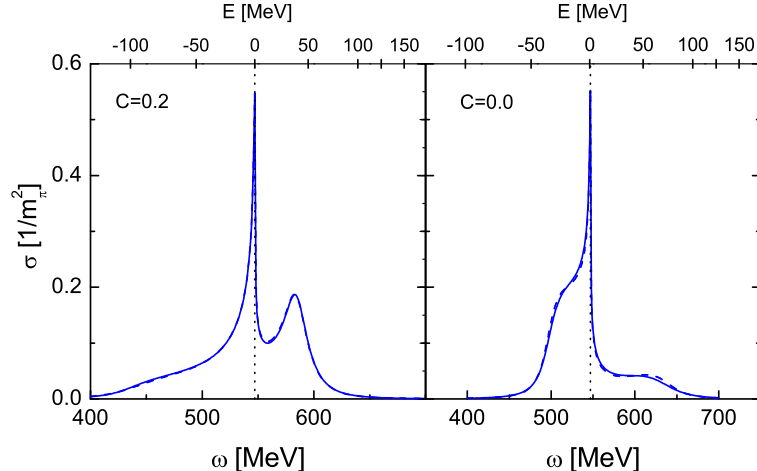


Fig. 6. The density-averaged nuclear response function (11) at zero momentum as a function of the eta meson energy, ω , (lower scale) and the binding energy $E = (\omega^2 - m_\eta^2)/2m_\eta$ (upper scale) calculated for $C = 0.2$ (left panel) and $C = 0$ (right panel). Dashed lines correspond to the constant N^* width and solid lines to the energy and density dependent width. The vertical dotted lines mark the bare eta mass value.

spectrum of the eta meson produced in the nucleus interior. The difference between the $C = 0$ and $C = 0.2$ cases observed in Fig. 5 can be clearly seen also in the density-averaged response function. For $C = 0.2$ the bump in the continuum region is more pronounced and shifts to the higher energies, whereas the bump in the bound region slides down to lower energies and becomes smaller. Two modes repel each other stronger. Therefore, the response strength in the continuum region larger than that in the bound region can be a signal of the eta and $N^* - h$ level crossing in the nucleus.

It is worth noting that Eq. (11) is not applicable for calculation of the bound state parameters, since the Green function calculated in the infinite nuclear matter satisfy the boundary conditions different from those for the Green function in a finite nucleus. Therefore, the infinite-matter Green function does not have correct analytic properties as the actual *in-nucleus* Green function and direct identification of the bumps in Fig. 6 with the poles of the Green function is not possible. We note that identification of the density-averaged spectral function (11) with a local approximation of the actual in-nucleus Green function is not appropriate in regions where the nuclear density changes suddenly, like on the surface of a nucleus. Therefore, the cusp structures we observe in Fig. 6 can be only qualitatively compared to the actual spectra.

3.2 Bound and resonance states of eta-nucleus system

In order to understand better the bump structure of the response function shown in Fig. 6, we have to study poles of the eta-meson-nucleus scattering amplitude on the complex energy plane. The positions of the poles correspond to energies and widths of bound states of the eta and N^* - h modes in the nucleus. In practice, we search for the energy eigenvalues of the Klein-Gordon equation in the momentum space [60] for the eta meson with the angular momentum L in the nucleus:

$$p^2 \Psi(p) + \int_0^\infty p'^2 dp' v_L(p, p'; \omega) \Psi(p') = (\omega^2 - m_\eta^2) \Psi(p), \quad (13)$$

where Ψ is the wave function of the eta meson, and ω is the energy of the eta meson. The non-relativistic binding energy is defined as $E = (\omega^2 - m_\eta^2)/(2m_\eta)$. The potential $v_L(p, p'; \omega)$ in the momentum space is given by the Fourier transform of the energy-dependent self-energy $\Pi_\eta(\omega, 0; \rho(r))$ evaluated in Eq.(3) under the local density approximation:

$$v_L(p, p'; \omega) = \frac{2}{\pi} \int_0^\infty dr r^2 \Pi_\eta(\omega, 0; \rho(r)) j_L(p r) j_L(p' r) \quad (14)$$

with the spherical Bessel function $j_L(x)$. We put $k = 0$ since we consider slow eta excitations created for the recoilless kinematic conditions. The boundary conditions can be implemented more easily by considering the Green functions in Lippmann-Schwinger equation rather than the wave function in the Klein-Gordon equation. The corresponding Lippmann-Schwinger equation written as an operator equation in the momentum space is

$$\Psi = G^{(0)}(\omega) V(\omega) \Psi, \quad (15)$$

where the Green function $G^{(0)}$ and the potential V are given in the operator form by $G^{(0)}(\omega) = (\omega^2 - m_\eta^2 - \hat{p}^2 + i\epsilon)^{-1}$ and $V(\omega) = v_L(\hat{p}, \hat{p}'; \omega) \hat{p}'^2$. The explicit form of Eq.(15) is

$$\Psi(p) - \int_0^\infty dp' \frac{v_L(p, p'; \omega) p'^2}{\omega^2 - m_\eta^2 - p'^2 + i\epsilon} \Psi(p') = 0. \quad (16)$$

The bound state energies E , for which non-trivial solutions of the Lippmann-Schwinger equation (15) exist, follow from the secular equation

$$\det \left(1 - V(\sqrt{m_\eta^2 + 2m_\eta E}) G^{(0)}(\sqrt{m_\eta^2 + 2m_\eta E}) \right) = 0. \quad (17)$$

Some technical details of the calculations are given in Appendix A.

We discuss first the results obtained for $L = 0$ and $C = 0.2$. On the first Riemann sheet we find two poles at $E_1 = (-88.53 - i 11.54)$ MeV and $E_2 = (-74.13 - i 15.00)$ MeV, which correspond to the deepest bound η state in the ^{11}B nucleus and its first radial excitation, respectively. In the response function in Fig. 6 they manifest themselves as a small bump at about -80 MeV. On the first Riemann sheet there is another pole at $E = (6.40 - i 0.46)$ MeV. Located above the threshold, this pole stands for a virtual state, which is not seen in the spectrum as a resonance bump but causes the cusp at the threshold. On the second Riemann sheet there is a resonance state at $E = (61.02 - i 25.82)$ MeV, which shows up as a bump at ~ 50 MeV in the continuum region. Thus we conclude that the structure of the response function in Fig. 6 (left panel) contains signals of the two bound, one virtual and one resonance states. For the $C = 0$ case the analytical structure changes. The attraction weakens and there remains only one bound state at $(-22.18 - i 12.88)$ MeV on the first Riemann sheet. The other former bound state moves up and becomes a resonance at $(3.47 - i 54.78)$ MeV on the second Riemann sheet. The other resonance state on the second Riemann sheet is located now at somewhat smaller energy $(31.91 - i 54.79)$ MeV. The virtual state on the first Riemann sheet stays almost put at $(6.13 - i 0.69)$ MeV.

4 Formation spectra of η mesic nuclei

In this section we discuss the eta meson spectra in finite nuclei which can be observed in actual experiments. We consider nucleon pickup processes of the eta production on a nucleus. The (π, p) , $(d, ^3\text{He})$ and (γ, p) processes on nuclear targets have been already proposed as formation reactions of the eta-nucleus systems. The advantage of the nucleon pickup processes is that it is possible to create the eta meson in nucleus almost at rest (recoilless production). The momentum transfer can be reduced to zero by adjusting the incident particle energy. For the recoilless production, we have a selection rule for the total angular momentum of the produced meson and the nucleon-hole state inside the nucleus. Since at the recoilless kinematics no angular momentum is brought to the residual nuclear system, the substitutional states are largely enhanced. As the result the contributions of the different angular momenta among the mesonic and nuclear states are strongly suppressed. For the ^{12}C target case, the dominant contributions are provided by the $(0s_{1/2})_p^{-1} \otimes s_\eta$ and $(0p_{3/2})_p^{-1} \otimes p_\eta$ configurations, in which $(nL_S)_p^{-1} \otimes \ell_\eta$ denotes η -hole configuration with the η meson in the orbit ℓ and the proton hole in the orbit L with the spin S and the principal quantum number n , although the ground state configuration is $(0p_{3/2})_p^{-1} \otimes s_\eta$, which has different angular momenta for the η and proton-hole states [7].

In the experiments one observes the ejected nucleon in the final states inclusively and obtains the double differential cross sections $d^2\sigma/(d\Omega dE_N)$ as a functions of the energy, E_N , and the emission angle of the outgoing nucleon. Investigating the shape of the missing mass spectra, we may hope to extract the in-medium properties of the eta and N^* - h modes. Observing additional particles in the final state would help to confirm the creation of the eta and N^* - h states in the nucleus (see, e.g., proposal [16]).

Let us consider the $^{12}\text{C}(\gamma, p)^{11}\text{B}$ reaction as an example. The $(d, ^3\text{He})$ reactions were discussed in Refs. [7,10,11] and the (π, p) will be investigated in Ref. [58]. In the distorted-wave impulse approximation (DWIA) for the elementary process $\gamma p \rightarrow \eta p$, the differential cross section is given by the product of the elementary cross section and the nuclear response function $S(E)$:

$$\left(\frac{d^2\sigma}{d\Omega dE_N} \right)_{A(\gamma,p)(A-1)\otimes\eta} = \left(\frac{d\sigma}{d\Omega} \right)_{p(\gamma,p)\eta}^{\text{lab}} \times S(E_\gamma - E_N) . \quad (18)$$

where E_γ is the incident-photon energy. In (18) we assume that the two-body process $\gamma p \rightarrow \eta p$ dominates the eta production and the direct production of the N^* - h mode by the incident photon via the reaction $\gamma NN \rightarrow NN^*$ is subdominant.

We calculate the nuclear response function $S(E)$ following the Green function method for the hadrons in nuclei formulated in Ref. [59]. There the response function is given by the transition amplitudes $T_f(\mathbf{r})$ of $\gamma \rightarrow p^{-1}p\eta$ at the position \mathbf{r} and the Green function $G(E; \mathbf{r}, \mathbf{r}')$ of the eta meson in the residual nucleus:

$$S(E) = -\frac{1}{\pi} \text{Im} \int d\mathbf{r} d\mathbf{r}' \sum_f T_f^\dagger(\mathbf{r}) G(E - \Delta E_{j_p}; \mathbf{r}, \mathbf{r}') T_f(\mathbf{r}') , \quad (19)$$

where the summation is taken over the all possible final states and ΔE_{j_p} is the hole separation energy measured from the ground state of the daughter nucleus. After the summation of the nucleon spins the transition amplitude T_f is given by

$$T_f(\mathbf{r}) = \chi_f^*(\mathbf{r}) \xi_{1/2, m_s}^* \left[Y_{l_\eta}^*(\hat{r}) \otimes \psi_{j_p}(\mathbf{r}) \right]_{JM} \chi_i(\mathbf{r}) \quad (20)$$

with the proton-hole wave function ψ_{j_p} , the distorted waves χ_i and χ_j of the incident photon and the ejected proton, the eta meson angular wave function $Y_{l_\eta}(\hat{r})$ and the spin wave function $\xi_{1/2, m_s}$ of the ejected proton. JM denotes the total angular momentum of the η and proton-hole system. The Green

function $G(E; \mathbf{r}, \mathbf{r}')$ is written formally as

$$G(E; \mathbf{r}, \mathbf{r}') = \langle p^{-1} | \phi_\eta(\mathbf{r}) \frac{1}{E - H_\eta + i\epsilon} \phi_\eta^\dagger(\mathbf{r}') | p^{-1} \rangle \quad (21)$$

with the Hamiltonian containing the eta meson optical potential

$$U_\eta(\omega, r) = \frac{1}{2m_\eta} \Pi_\eta(\omega; \rho(r)). \quad (22)$$

In (21) ϕ_η^\dagger is the meson creation operator and $|p^{-1}\rangle$ is the residual nucleus state with a proton hole. The Green function $G(E; \mathbf{r}, \mathbf{r}')$ given in Eq.(21) is calculated by solving the Klein-Gordon (or Schrödinger) equation with appropriate boundary conditions. In general, the Green function can depend on the nuclear states and give transitions between different states. Here we have assumed that these state dependence and transitions are negligibly small.

The density averaged spectral function (11) is related to the actual response function (19) in the following way: since at the recoilless production the eta meson created in the nucleus moves slowly, it cannot propagate a long distance being absorbed rather soon. In this case the in-nucleus Green function $G(E; \mathbf{r}, \mathbf{r}')$ given in Eq.(21) can be approximated as

$$G(E; \mathbf{r}, \mathbf{r}') \simeq \delta(\mathbf{r} - \mathbf{r}') G_\eta(E; \rho(r)), \quad (23)$$

where $G_\eta(E; \rho(r))$ is the Green function for infinite nuclear matter obtained in the local density approximation. Neglecting the distortion effects on the incident photon and the ejected proton in the transition amplitude $T_f(\mathbf{r})$ in Eq.(20) and replacing the product of the hole wave-functions, $\psi_{j_p}^\dagger(\mathbf{r})\psi_{j_p}(\mathbf{r})$ by the density distribution $\rho(r)$ after the summation of the final states, we obtain an approximate response function

$$S(E) \propto \int dr r^2 \rho(r) \Im G_\eta(E; \rho(r)). \quad (24)$$

This is the density weighted in-medium Green function introduced in (11) except for the normalization. According to the above argument, the approximate spectral function is close to the in-nucleus spectral function obtained by solving the Klein-Gordon equation, if the local density approximation is good enough. In the proceeding calculations of the formation spectra of eta mesic nuclei we use the complete in-nucleus Green function (21).

The calculated formation spectra of the eta meson in the (γ, p) reaction with the ^{12}C target are shown in Fig. 7. The incident photon energy $E_\gamma = 950$ MeV

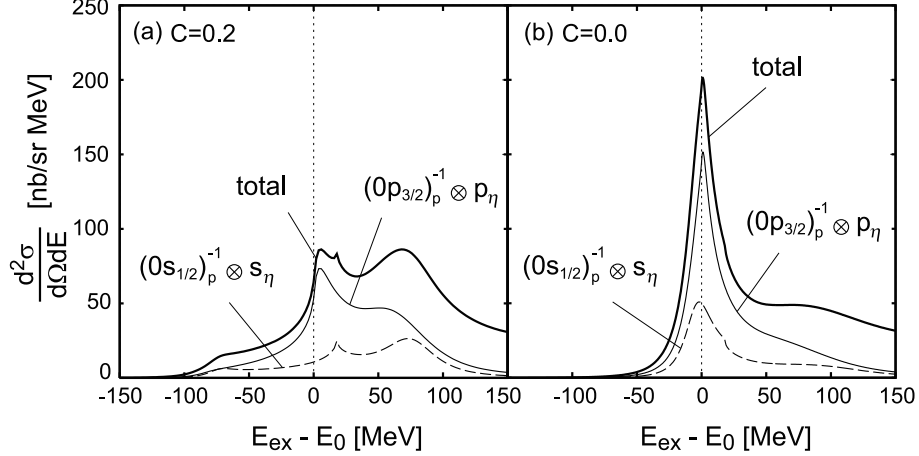


Fig. 7. Formation spectra of the eta meson in the (γ, p) reaction on the ^{12}C target at $E_\gamma = 950$ MeV as a function of the energy of the proton, E_{ex} , emitted at zero angle. The proton energy is counted from the eta production threshold E_0 . The left and right panels are the formation spectra calculated in the chiral doublet model (the naive model) with $C = 0.2$ and $C = 0.0$, respectively.

is chosen so that the recoilless condition is satisfied for the bare eta mass. We plot the missing mass spectra in the energy range wider than those shown in Refs. [10,11,12] to see the global structure of the spectra and to be able to identify the bound and resonance states discussed in the previous section. The energy of the emitted proton is counted from the creation threshold of the vacuum eta mass. The left (right) side of the threshold corresponds to the bound (continuum) energy region. We have calculated the sum of all contributions from the possible configurations of the proton-hole states, $s_{1/2}$ and $p_{3/2}$, and the eta states with $l = 0$ to 6. The total spectra are dominated by two contributions from the $(0s_{1/2})_p^{-1} \otimes s_\eta$ and $(0p_{3/2})_p^{-1} \otimes p_\eta$ configurations due to the selection rule at the recoilless kinematics. The separation energies of the s state protons are taken into account in the spectra. The formation spectra are discussed in more details in Refs. [10,11,12].

The missing mass spectrum calculated in the chiral doublet model with $C = 0.2$ and shown on the left panel in Fig.7 has the richer structure than the spectrum obtained with $C = 0.0$, when no level crossing takes place. We compare the sub-component $(0s_{1/2})_p^{-1} \otimes s_\eta$ in Fig.7 with the response function plotted in Fig. 6. The centrifugal potentials are not taken into account in the latter function. We find that still the approximated response function reproduces well the bump structure of the spectrum obtained in the full calculation with the actual Green function. (Exception is the eta threshold energies, when the contributions from the eta meson on the surface of the residual nucleus are dominated.) This is because the distortion factors have smooth energy dependence and the initial photon is less distorted. Thus, the conclusions drawn in the previous section for the approximated spectra hold also for the actual formation spectra. Namely, the bump structures correspond to the bound and

resonance states. For the $C = 0.2$ case, we have found the two bound states and one resonance state. They correspond to the small bump around $E = -80$ MeV and the pronounced peak in $E = 80$ MeV, respectively.

We conclude that the more pronounced bump structure in the continuum energy region can be a signal of the level crossing. Note that the recoilless kinematics largely suppresses the second bound state (the radial excited state) in the spectrum, since there are no proton-hole states in ^{11}B to satisfy the selection rule with the second s state of the eta meson.

5 Conclusion

We have investigated the eta-nucleus system, paying attention to the $N(1535)$ -nucleon-hole mode in nuclear medium. We have found that the N^*-h contribution is important for the eta meson in nuclear matter and induces strong energy dependence of the eta self-energy. We have also shown that reduction of the difference between the masses of N^* and N as a result of the medium effects leads to level crossing of the eta and N^*-h modes, and modification of the eta spectral function. The change of the spectral function is clearly seen in formation spectra of eta nuclei.

Acknowledgments

E.E.K. thanks the Yukawa Institute for hospitality. This work is supported by the Grant-in-Aid for the 21st Century COE "Center for Diversity and Universality in Physics" from the Ministry of Education, Culture, Sports, Science and Technology (MEXT) of Japan. The work of D.J. was also partially supported by the Grant for Scientific Research (No. 18042001) from MEXT. The work of E.E.K. was supported in part by the US Department of Energy under contract No. DE-FG02-87ER40328. The work of H.N. was supported by Japan Society for the Promotion of Science (No. 18-8661). This work is part of Yukawa International Program for Quark-Hadron Sciences.

A Appendix

The numerical solution of the equation (16) is performed by the method suggested in Ref. [60]. The integral equation is written as a matrix equation in

momentum space by replacing momentum integral with a sum over N grid points:

$$\Psi_m = \sum_{n=1}^N M_{mn} \Psi_n \quad (\text{A.1})$$

with

$$M_{mn} = V_{mn}(\omega) G_n^{(0)}(\omega) W_n, \quad (\text{A.2})$$

where W_n is a weight function for the discretization of the integral and

$$V_{mn}(\omega) = v_L(p_m, p_n; \omega) p_n^2, \quad (\text{A.3})$$

$$G_n^{(0)}(\omega) = \frac{1}{\omega^2 - m_\eta^2 - p_n^2 + i\epsilon}. \quad (\text{A.4})$$

At the end we search for zeros of the determinant of the $N \times N$ matrix:

$$\det(1 - M) = 0 \quad (\text{A.5})$$

for the complex binding energy $E = (\omega^2 - m_\eta^2)/(2m_\eta)$.

In this method, one can choose properly the boundary conditions of the scattering equation. For the first Riemann sheet solutions, we just solve Eq.(A.5) for a complex E . For the second Riemann sheet, where we can obtain resonance solution, one should treat $i\epsilon$ in the Green function $G^{(0)}$ given in Eq.(A.4) before going to the complex plane. This can be done as follows. The integral in the left hand side of Eq.(16) can be written in terms of principle value integral as

$$\Psi(p) = P \int_0^\infty dp' \frac{v_L(p, p'; \omega) p'^2}{\omega^2 - m_\eta^2 - p'^2} \Psi(p') - i \frac{1}{2} \pi k v_L(p, k; \omega) \Psi(k), \quad (\text{A.6})$$

where k is a complex momentum $k^2 = \omega^2 - m_\eta^2 = 2m_\eta E$ on the second Riemann sheet. As discussed in Ref. [61], these terms are implemented to the matrix formulation by extending the matrix M in (A.5) and defining an extra grid point $p_{N+1} = k$ as

$$M_{N+1,n} = v_L(k, p_n; \omega) \frac{W_n p_n^2}{k^2 - p_n^2}, \quad (\text{A.7})$$

$$M_{n,N+1} = v_L(p_n, k; \omega) \left(\sum_{m=1}^N \frac{-W_m k^2}{k^2 - p_m^2} - i \frac{1}{2} \pi k \right), \quad (\text{A.8})$$

$$M_{N+1,N+1} = v_L(k, k; \omega) \left(\sum_{m=1}^N \frac{-W_m k^2}{k^2 - p_m^2} - i \frac{1}{2} \pi k \right). \quad (\text{A.9})$$

References

- [1] Q. Haider and L.C. Liu, Phys. Lett. B **172** (1986) 257; L.C. Liu and Q. Haider, Phys. Rev. C **34** (1986) 1845; Q. Haider and L.C. Liu, Phys. Rev. C **36** (1987) 1636.
- [2] R.S. Bhalerao and L.C. Liu, Phys. Rev. Lett. **54** (1985) 865.
- [3] C.J. Batty, E. Friedman, and A. Gal, Phys. Rept. **287** (1997) 385; *ibid* **452** (2007) 89.
- [4] A. Sibirtsev, J. Heidenbauer, J.A. Niskanen, and U.-G. Meißner, Phys. Rev. C **70** (2004) 047001.
- [5] M. Kohno and H. Tanabe, Phys. Lett. B **231** (1989) 219; Nucl. Phys. A **519** (1990) 755.
- [6] H.C. Chiang, E. Oset, and L.C. Liu, Phys. Rev. C **44** (1991) 738.
- [7] R. S. Hayano, S. Hirenzaki, and A. Gillitzer, Eur. Phys. J. A **6** (1999) 99.
- [8] K. Tsushima, D. Lu, A.W. Thomas, and K. Saito, Phys. Lett. B **443** (1998) 26.
- [9] C. Garcia-Recio, T. Inoue, J. Nieves, and E. Oset, Phys. Lett. B **550** (2002) 47.
- [10] D. Jido, H. Nagahiro, and S. Hirenzaki, Phys. Rev. C **66** (2002) 045202; Nucl. Phys. A **721** (2003) 665.
- [11] H. Nagahiro, D. Jido, and S. Hirenzaki, Phys. Rev. C **68** (2003) 035205.
- [12] H. Nagahiro, D. Jido, and S. Hirenzaki, Nucl. Phys. A **761** (2005) 92.
- [13] R.E. Chrien *et al.*, Phys. Rev. Lett. **60** (1988) 2595.
- [14] J. Berger *et al.*, Phys. Rev. Lett **61** (1988) 919.
- [15] J.D. Johnson *et al.*, Phys. Rev. C **47** (1993) 2571.
- [16] G.A. Sokol and V.A. Triasuchev, Sov. Physics- Lebedev Insitute Report **4** (1991) 23.
- [17] G.A. Sokol, T.A. Aibergenov, A.V. Kravtsov, A.I. L'vov, and L.N. Pavlyuchenko, Fizika B **8** (1999) 85; G.A. Sokol, A.I. L'vov, and L.N. Pavlyuchenko, nucl-ex/0106005.
- [18] M. Pfeiffer *et al.*, Phys. Rev. Lett. **92** (2004) 252001.
- [19] Ch. Hanhart, Phys. Rev. Lett. **94** (2005) 049101.

- [20] C. Wilkin *et al.*, Arxiv:0707.1489 [nucl-ex] (2007).
- [21] V.A. Baskov *et al.*, Arxiv:nucl-ex/0306011.
- [22] M.K. Anikina *et al.*, Arxiv:nucl-ex/0412036.
- [23] V. Jha *et al.* [GEM Collaboration], Int. J. Mod. Phys. A **22** (2007) 596.
- [24] H. Toki, S. Hirenzaki, and T. Yamazaki, Nucl. Phys. A **530** (1991) 679; S. Hirenzaki, H. Toki, and T. Yamazaki, Phys. Rev. C **44** (1991) 2472.
- [25] H. Gilg *et al.*, Phys. Rev. C **62** (2000) 025201; K. Itahashi *et al.*, *ibid.* **62** (2000) 025202.
- [26] H. Geissel *et al.*, Phys. Rev. Lett. **88** (2002) 122301.
- [27] P. Kienle and T. Yamazaki, Phys. Lett. B **514** (2001) 1; H. Geissel *et al.*, *ibid.* **549** (2002) 64; K. Suzuki *et al.*, Phys. Rev. Lett. **92** (2004) 072302.
- [28] T. Yorita *et al.*, Phys. Lett. B **476** (2000) 226; T. Kinoshita *et al.*, Phys. Lett. B **639** (2006) 429.
- [29] T. Maruyama and S. Chiba, Prog. Theor. Phys. **111** (2004) 229.
- [30] J. Lehr, M. Post, and U. Mosel, Phys. Rev. C **68** (2003) 044601.
- [31] B. Krusche *et al.*, Phys. Rev. Lett. **74** (1995) 3736; M. Benmerrouche and N.C. Mukhopadhyay, *ibid.* **67** (1991) 1070; Phys. Rev. D **51** (1995) 3237.
- [32] L. Tiator, C. Benhold, and S.S. Kamalov, Nucl. Phys. A **580** (1994) 455.
- [33] W. Grein and P. Kroll, Nucl. Phys. A **338** (1980) 332.
- [34] G.A. Christos, Z. Phys. C **21** (1983) 83; Phys. Rev. D **35** (1987) 330.
- [35] C. DeTar and T. Kunihiro, Phys. Rev. D **39** (1989) 2805.
- [36] T. Hatsuda and M. Prakash, Phys. Lett. B **224** (1989) 11.
- [37] D. Jido, N. Kodama and M. Oka, Phys. Rev. D **54** (1996) 4532.
- [38] D. Jido, Y. Nemoto, M. Oka, and A. Hosaka, Nucl. Phys. A **671** (2000) 471; D. Jido, M. Oka, and A. Hosaka, Prog. Theor. Phys. **106** (2001) 873.
- [39] H. Kim, D. Jido and M. Oka, Nucl. Phys. A **640** (1998) 77.
- [40] N. Kaiser, P.B. Siegel and W. Weise, Phys. Lett. B **362** (1995) 23.
- [41] N. Kaiser, T. Waas and W. Weise, Nucl. Phys. A **612** (1997) 297.
- [42] M.F.M. Lutz and E.E. Kolomeitsev, Nucl. Phys. A **700** (2002) 193; E.E. Kolomeitsev and M.F.M. Lutz, Phys. Lett. B **585** (2004) 243.
- [43] T. Inoue, E. Oset, and M. Vicente Vacas, Phys. Rev. C **65** (2002) 035204.
- [44] T. Waas and W. Weise, Nucl. Phys. A **625** (1997) 287.

- [45] A. Ramos and E. Oset, Nucl. Phys. **A671** (2000) 481.
- [46] M.F.M. Lutz and C.L. Korpa, Nucl. Phys. A **700** (2002) 309
- [47] M.F.M. Lutz, C.L. Korpa, and M. Möller, Arxiv:0707.1283 [nucl-th].
- [48] T. Inoue and E. Oset, Nucl. Phys. A **710** (2002) 354.
- [49] T. Hatsuda, T. Kunihiro, and H. Shimizu, Phys. Rev. Lett. **82** (1999) 2840;
D. Jido, T. Hatsuda, and T. Kunihiro, Phys. Rev. D **63** (2000) 011901.
- [50] P. Costa, M. C. Ruivo, and Yu. L. Kalinovsky, Phys. Lett. B **560** (2003) 171;
P. Costa, M.C. Ruivo, C.A. de Sousa, and Yu.L. Kalinovsky, Phys. Rev. D **70**
(2004) 116013.
- [51] H. Nagahiro, M. Takizawa, and S. Hirenzaki, Phys. Rev. C **74** (2006) 045203.
- [52] Ch. Sauer mann, B. Friman, and W. Nö renberg, Phys. Lett. B **341** (1995) 261.
- [53] C. Wilkin, Phys. Rev. C **47** (1993) 938.
- [54] M. Batinic, I. Slaus, and A. Svarc, Phys. Rev. C **52** (1995) 2188.
- [55] M. Arima, K. Shimizu, and K. Yazaki, Nucl. Phys. A **543** (1992) 613.
- [56] Ch. Sauer mann, Diplom thesis, TH Darmstadt (1993).
- [57] A.B. Migdal, Rev. Mod. Phys. **50** (1978) 107.
- [58] H. Nagahiro, D. Jido, and S. Hirenzaki, in preparation.
- [59] O. Morimatsu and K. Yazaki, Nucl. Phys. A **435** (1985) 727; *ibid.* **483** (1988)
493; Prog. Part. Nucl. Phys. **33** (1994) 679.
- [60] R.H. Landau, Phys. Rev. C **27** (1983) 2191.
- [61] M.I. Haftel and F. Tabakin, Nucl. Phys. A **158** (1970) 1.